sustainability

MDPI

Article

Multi-Factor Design for a Vacuum Ejector Improvement by In-Depth Analysis of Construction Parameters

Llorenç Macia *, Robert Castilla, Pedro Javier Gamez-Montero and Gustavo Raush

CATMech—Centre for Advanced Technologies in Mechanics, Universitat Politecnica de Catalunya, Catalunya, ES-08222 Terrassa, Spain

* Correspondence: llorenc.macia@upc.edu

Abstract: A vacuum supersonic ejector is an indispensable pneumatic device placed in nearly all industrial production lines. This device, also called a zero-secondary flow ejector, is characterized by the maximum entrained flow and the minimum secondary pressure. Numerical simulations were carried out by means of the CFD toolbox OpenFOAM v8 and its solver HiSA, which uses the AUSM+up upwind scheme. A single-factor analysis of eight parameters was performed to find how the ejector's performance was enhanced or decreased, while other parameters were fixed. Four parameters were subject to further analysis to find the geometry that improves the standalone performance of the ejector. The mixing chamber length is the parameter that most improves its performance; alone it leads to a 10% improvement. A multi-factor analysis, based on a fractional factorial design, is carried out with the four relevant parameters. Results indicate that the multi-factor analysis enhances the performance of the ejector by 10.4% and the mixing chamber length is the factor that most influences the improvement. Although a multi-factor design improves the performance, no significant relevance has been detected with respect to the mixing chamber length improvement alone. The improved performance of this device leads to a reduction in operating time and, as a consequence, results in significant energy savings.

Keywords: vacuum ejector; OpenFOAM; CFD; HiSA; compressible flow; multi-factor design; nozzle; supersonic

Citation: Macia, L.; Castilla, R.; Gamez-Montero, P.J.; Raush, G. Multi-Factor Design for a Vacuum Ejector Improvement by In-Depth Analysis of Construction Parameters. *Sustainability* **2022**, *14*, 10195. https://doi.org/10.3390/su141610195

Academic Editor: Michael O'Sullivan

Received: 31 May 2022
Accepted: 14 August 2022
Published: 17 August 2022

1. Introduction

Large-scale production is one of the characteristics of modern societies. All over the world there are factories and, in them, there are production lines. In almost every one of them, there is a robot that handles the product at some stage of its production. It is at this point that the ejectors come into their own. There are different approaches when handling a product, but a vacuum ejector with suction cups is one of the most common [1].

Therefore, the most important characteristics of a vacuum generator or vacuum ejector are the maximum entrained flow and the minimum secondary pressure, or maximum vacuum. The higher the entrained flow and the vacuum achieved, the more efficient handling of the product. This is the reason that motivated the authors of this work to investigate and improve the performance of this device.

A vacuum ejector works with compressed air as a pneumatic component, and it exploits the Venturi effect.

Figure 1 shows a simplified schematic of the vacuum ejector in order to show how it works.

The primary flow, which is supersonic, is produced by the pressure difference between the compressed air at the primary inlet and the atmospheric pressure at the outlet. The primary flow carries the entrained flow, also called secondary flow, since it comes from the secondary inlet.

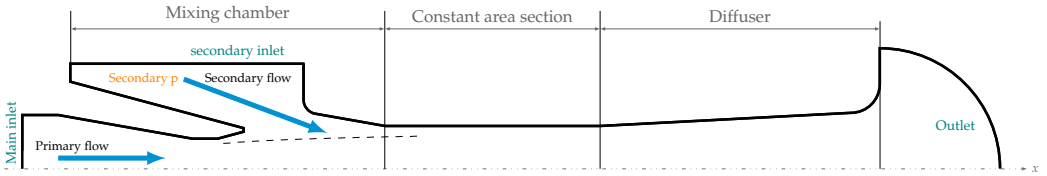

Figure 1. Diagram of ejector geometry with internal geometry showing the two most important characteristics. The flow direction is from the left (main inlet) to the right (outlet).

The pressure at the secondary inlet will decay to the minimum pressure value, also known as the maximum vacuum, that the ejector can produce.

These two main features depend exclusively on the internal geometry of the ejector since there are no moving parts. Thus, to increase the performance indices of the vacuum ejector, the internal geometry needs to be changed.

There are two different options when manufacturing a vacuum ejector. The first configuration consists of straight concatenated nozzles. Within this type, there are two categories: the constant-area mixing ejector [2,3] and the constant-pressure mixing ejector. A great amount of literature has been published on the latter category, for example [4,5].

The second type is made of concatenated Laval nozzles in order to adapt the nozzles to a specific back pressure [6].

A comparable body of research articles in the past [7] has been written on studies of an optimal single-factor design for a supersonic ejector. Jingming Dong et al. [8] studied the influence of one geometrical parameter of a steam ejector. They realized that the performance can be improved by changing the geometrical values. Jia Yan et al. [9,10] worked in changing geometrical values and studied a single-factor enhancement, but not a multi-factor enhancement. The same team carried out another project [10] where they tried to enhance the entrained ratio through some geometrical changes to the design.

Hailun Zhang et al. [11] found that friction has a significant influence on the performance of the ejector and the efficiency of its components. This factor has been deliberately left aside because is going to be considered as a new parameter in the multi-factor design in a future work.

An important body of research is also based on experimental work [12,13]. Ramesh et al. [14,15] performed an experimental study of the angle for the mixing chamber, leading to a significant enhancement of the performance of the ejector.

Ejectors are a component in most cooling cycle solar installations. VuVan Nguyen [16] worked in applying a variable geometry for an ejector. Although they found some enhancement, their purpose rather differs from the present one, since they consider a refrigerator nozzle and not a vacuum ejector. Therefore, in their work it is not a priority to improve the secondary pressure of the device. Fahid Riaz et al. [17] integrated an ejector in their cooling cycle-driven model in pursuance of improving their COP for the model.

In the past, similar research to that discussed in this paper has been performed by other authors. José Sierra-Pallares et al. [18] carried out a similar study but with different geometry and a different fluid. They changed the back pressure since they were dealing with a refrigerator ejector.

Yifei Wu et al. [19] have done similar work improving the performance of a steam ejector through a multi-factor study of all internal parameters. Differences arise because they consider a refrigerator nozzle.

Since they deal with more levels per parameter, they optimize the structural parameters through an orthogonal test, not by a fractional factorial design.

The performance of a vacuum ejector is considered to be improved by an increase in the maximum secondary flow rate and a decrease in the minimum final secondary pressure. The secondary flow, or entrained flow, is normalized by the primary flow, as shown in (1).

$$\mu = \frac{\dot{m}_s}{\dot{m}_p} \tag{1}$$

The secondary pressure is normalized with the atmospheric pressure, as shown in (2).

$$p_s^* = \frac{p_s}{p_a} \tag{2}$$

Once the individual behaviour of these two characteristics has been analysed, both will be added together for a measure of overall improvement. The aim of this paper is to find the internal geometry of a vacuum ejector that enhances its performance in terms of secondary flow and pressure.

First, a single-factor in-depth investigation was carried out on all the geometrical parameters in th design of an ejector, to analyse the enhancement or deterioration of its performance in terms of secondary flow and pressure. A single-factor evaluation of the improvement in the performance per parameter was implemented. Then the fractional factorial design was implemented to find the influence of multi-factor influences in the overall enhancement of the performance.

The present paper is organized as follows. Section 2 describes the single-factor evaluation, the numerical simulations run in this paper and the multi-factor design is presented. Section 3 presents the main results obtained, while in Section 4 these results are discussed, and finally, conclusions are drawn.

2. Materials and Methods

2.1. Numerical Method

2.1.1. The Solver

The numerical simulation toolbox employed in this work was OpenFOAM [20] with the High-Speed Aerodynamic solver (HiSA) [21]. The solver models compressible transonic and supersonic flows, through a density-based approach, and allows a resolution of numerical discontinuities, including formation and propagation of shock waves [22]. HiSA is an implicit density-based solver designed for compressible flows. Implicit solvers allow simulations with high CFL numbers with more stability [23].

HiSA uses two flux interpolation schemes, the Harten–Lax–van Leer contact solver and the advection upstream splitting method, to improve the computation of the face fluxes over a wider range of speed regimes. This approach involves solving the system of equations using a generalized minimum residual method with lower–upper symmetric Gauss–Seidel preconditioning. The solver allows for the definition of non-reflective far-field boundary conditions [24], which is essential when modelling transonic external flows with shock waves. Furthermore, it is ensured that truncating the numerical domain does not influence the development of the flow. A second-order least-squares approach is used to calculate the gradient terms. It leads to faster convergence and a more stable simulation compared to a Gauss linear scheme. Divergence terms are evaluated using a second-order Gauss scheme with linear interpolation. An orthogonal scheme is used for the computation of surface normal gradients and Laplacian schemes, which can be used on meshes of low non-orthogonality, which is the case for the current study, by using a very good hexahedral parametric mesh. Gradient limiters for pressure, temperature, velocity, and turbulent quantities are defined to improve stability and convergence.

Hence, HiSA solves the transient Navier–Stokes equations for compressible mass-flow, momentum and energy:

$$\frac{\partial \rho}{\partial t} + \frac{\partial}{\partial x_i}\rho u_i = 0 \tag{3}$$

$$\frac{\partial}{\partial t}\rho u_j + \frac{\partial}{\partial x_i}\rho u_i u_j = -\frac{\partial p}{\partial x_i} + \frac{\partial}{\partial x_i}\sigma_{ij} \tag{4}$$

$$\frac{\partial}{\partial t}\rho E + \frac{\partial}{\partial x_i}\rho E u_i = -\frac{\partial u_i p}{\partial x_i} + \frac{\partial}{\partial x_i}\left(u_i \sigma_{ij} + k\frac{\partial T}{\partial x_j}\right) \tag{5}$$

with

$$\sigma_{ij} = \mu_0 \left(\frac{\partial u_i}{\partial x_j} + \frac{\partial u_j}{\partial x_i} - \frac{2}{3} \frac{\partial u_k}{\partial x_k} \delta_{ij} \right) \tag{6}$$

where μ_0 is the dynamic viscosity of the selected fluid.

The Navier–Stokes equations are solved along with the equation for perfect gases

$$p = \rho R' T \tag{7}$$

where $E = c_v T + \frac{1}{2}|\mathbf{u}|^2$, c_v is the specific heat at constant volume and R' is the constant for the gas. The turbulence model used is k-ω SST, since it was reported to give better results for the type of simulation by comparison with k-ϵ, k-ϵ realizable and stress-ω Reynolds stress model, as reported in Federico Mazzelli et al. [25].

2.1.2. The Mesh

In the present paper, a similar approach to [1] in terms of the mesh has been followed. A 2D axis-symmetric mesh has been used with wedge construction. The mesh is created with blockMeshDict, a powerful tool for structured block mesh construction. Nevertheless, when dealing with complex geometry it is very convenient to use ofblockmeshdictHelper [26], an object-oriented library for Python, that assists in the parametrization of the geometry.

Critical geometrical parameters have been used to define the mesh, see Figure 2.

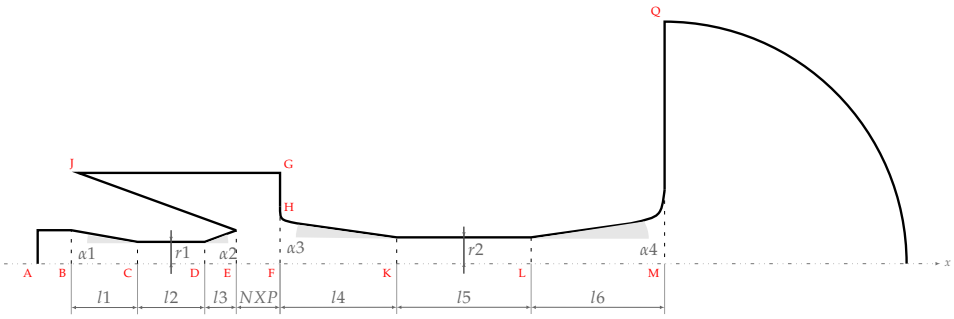

Figure 2. Relevant geometrical parameters in the design of a Vacuum ejector.

The mesh is constructed for two concatenated nozzles, as was previously explained in the introduction section. The horizontal length NXP is the distance between the two nozzles, also known as the nozzle exit position. The literature suggests [27–29] that it is an important geometrical value and requires further investigation.

The first two horizontal geometrical parameters, $l1$ and $l2$, do not contribute significantly to the two relevant ejector characteristics, as explained in Section 1, therefore, they are neglected. The first angle, $\alpha 1$, is neglected since it will only lengthen the primary inlet. The last angle, $\alpha 4$, is also neglected since it will only lengthen the exit to the outlet. The literature suggests [19] that $r1$ does not play any significant role since the secondary flow is normalized with the primary flow.

As a result of this preliminary study, eight geometrical parameters were considered relevant for further study.

2.1.3. Boundary Conditions

The operating fluid selected is air, assumed to be a perfect gas. The thermophysical properties of air are listed in Table 1, which were treated as constant except for density, which is calculated according to Equation (7). The viscosity was treated as constant since there are no relevant temperature gradients.

Table 1. Thermophysical properties of air.

Property	Value
Dynamic viscosity, μ_0	1.8 (kg/s m)
Specific heat capacity, C_p	1004.5 (J/kg K)
Molecular mass, M	28.96 (g/mol)
Prandtl number, P_r	0.7 (-)

Two types of simulations were performed in order to find the enhancement for the two characteristics of a vacuum ejector, as explained in the introduction section. In the first type, the secondary pressure was fixed with a constant value of 0.1 MPa and the flow rate is computed. In the second type, the gradient of secondary pressure is fixed at zero and the minimum value is eventually obtained. Table 2 lists the different types of patches used in each type of simulation.

Table 2. OpenFOAM patches names and boundary condition values per simulation type.

Simulation Type	**Entrained Flow**		**Secondary Pressure**	
Patch Name	***p* Patch Type**	**Pressure (MPa)**	***p* Patch Type**	**Pressure (MPa)**
Main Inlet	uniformTotalPressure	0.7	uniformTotalPressure	0.7
Secondary Inlet	totalPressure	0.1	zeroGradient	–
Outlet	characteristicFarfieldPressure	0.1	characteristicFarfieldPressure	0.1

Detailed analyses have shown y^+ values with a maximum of 55, a minimum of 10 and an average of 35. Instead of fully resolving the boundary layer, wall functions are employed in this solver to limit the required computational resources, as explained in the literature [30]. Hence, two boundary conditions are required in the logarithmic layer: *kqRWallFunction* and *omegaWallFunction*.

The temperature was set as the standard atmospheric total temperature of 293 K, and the boundary condition used in all boundaries was *totalTemperature*.

2.1.4. Simulation Performance

A grid convergence study was performed to check the quality of the mesh [1]. The study was carried out following the recommendations of Celik et al. [31] and, hence, the variation in cell size is about 30%. Three variables were considered for the grid convergence study: primary and secondary flow rates for atmospheric pressure in the secondary inlet (in other words, maximum secondary flow rate), and minimum pressure in the secondary inlet. Data are presented in Table 3.

Table 3. Data for grid convergence study.

Mesh	**Number of Cells**	$\dot{m}_p$ **(kg/s)**	$\dot{m}_s$ **(kg/s)**	$p_{s,\min}$ **(kPa)**
Coarse mesh	13,000	0.00945	0.00932	21.57
Study mesh	20,300	0.00946	0.00938	21.73
Fine mesh	29,250	0.00948	0.00936	21.90

The grid convergence analysis gives a relative error of 0.4% for the secondary flow rate and, hence, the result is $\dot{m}_s = (93.5 \pm 0.4) \times 10^{-3}$ kg/s.

The conclusions of this study [1] are that the solver and the mesh capture the discontinuities of the supersonic shock waves and reproduce the same flow rates as in the experiments.

A speedUp test was performed to find the number of CPUs for running each simulation. Although Figure 3 shows a better performance for all multiples of two, in the

present work, it has been decided to work with four CPUs for the sake of computational resources utilization.

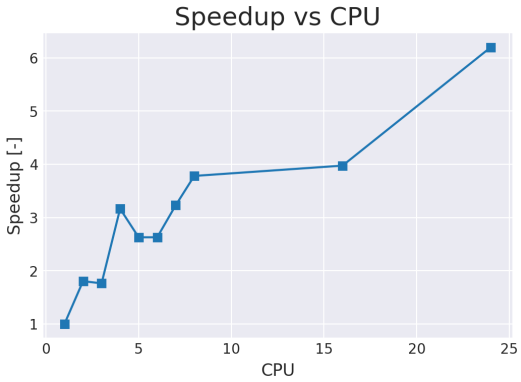

Figure 3. Analysis of the speedUp per CPU performance.

2.2. Factor Evaluation Design of the Numerical Simulations

2.2.1. Criterion for Improvement

As mentioned in Section 1, the enhancement of the performance of the vacuum ejector is obtained by improving the entrained flow rate and the secondary pressure of the ejector. A new geometry that does not meet either a pressure improvement or a flow rate enhancement will not be considered. Afterwards, the geometry that most enhances the overall performance is chosen.

The overall enhancement, Equation (8), is calculated as a sum of both partial enhancements.

$$O_E = SP_E + FR_E \tag{8}$$

where O_E is the overall enhancement, SP_E is the secondary pressure enhancement and FR_E is the secondary flow rate enhancement.

2.2.2. Single-Factor Evaluation Method

A single-factor evaluation of improvement of the ejector's performance was carried out: while only one parameter changed, the rest were fixed.

Every relevant parameter was discussed in Section 2.1.2. For each relevant parameter, two new geometries have been created.

The first geometry has a $+1/3$ increment of the reference value of the parameter and the second geometry has a $-1/3$ diminution. The geometrical modification is a compromise between span and numerical sensitivity.

These two new geometries are tested with the simulations described in Section 2.1.3 and their results evaluated according to the criterion for improvement, explained in Section 2.2.1.

The parameters that meet the improvement criteria were further investigated by creating new geometries with the same increase. As long as the new geometries meet the criteria, the same procedure is followed.

To create new geometries, the parameter can be increased unlimitedly from its reference value, but it can only be decreased up to a maximum of -100% of it.

Once the criterion fails to be met, the results are plotted and the geometry with the best enhancement is proposed.

2.2.3. Multi-Factor Design

With all geometrical parameters studied, a combination of design parameters is proposed in order to analyse the multi-factor influence on the overall enhancement of the ejector.

Each parameter has two levels: the first is the geometry with the reference value and, the second, is the geometry with the single-factor value found that enhances the performance. With these selected parameters, along with their two levels, a multi-factor analysis is required to find the combined overall enhancement. There are several methods for combining these parameters.

A full factorial design combines all the parameters and allows us to study their individual influence on the overall improvement. The full factorial design was discarded and a fractional factorial design was used, inspired by the Taguchi method [32]. A fractional factorial design reduces costs and computational resources.

The Taguchi method proposes a reduction of the total number of combinations in order to study the influence of multiple factors on the improvement of overall performance. It is named fractional factorial design instead of the Taguchi method because the latter involves topics unrelated to the present paper.

3. Results

3.1. Influence of Parameters on Overall Improvement

3.1.1. Analysis of the Eight Relevant Initial Parameters

After running the simulations with the eight relevant parameters, the results shown in Figure 4 were obtained. In Figure 4 the flow rate enhancement is shown in blue, the pressure enhancement in orange and the overall enhancement, calculated in Equation (8), in green.

For the parameter $\alpha 2$, both new geometries show a deterioration of the overall performance. Thus, this parameter was discarded and no further study using it was made.

For the parameter $\alpha 3$, new geometry $+1/3RV$ shows a deterioration of the performance. Thus, no further study was made. However, the case $-1/3RV$ shows the improved performance of the three characteristics. For this parameter further investigations were made.

For the parameter NXP, the new geometry $-1/3RV$ shows a deterioration of the performance. Thus, no further study was made. However, the case $+1/3RV$ geometry shows the improved performance of the three characteristics. For this parameter further investigations were made.

For the parameter $r2$, both new geometries show a deterioration of the overall enhancement. Thus, this parameter was discarded and no further study was made.

For the parameter $l3$, both new geometries show a deterioration of the overall enhancement. Although the $-1/3RV$ geometry shows an improvement in the overall enhancement, it fails the optimization criterion of enhancement of the three characteristics. Thus, this parameter was discarded and no further study was made.

For the parameter $l4$, the new value $+1/3RV$ shows a deterioration of the overall enhancement. Thus, no further study was made. However, the $-1/3RV$ geometry shows the improved performance of the three characteristics. For this parameter further investigations were made.

For the parameter $l5$, the new geometry $+1/3RV$ shows a deterioration of the overall enhancement. Then, no further study was made. However, the case $-1/3RV$ shows the improved performance of the three characteristics. For this parameter further investigations were made.

For the parameter $l6$, both new geometries show a deterioration of the overall enhancement. Thus, this parameter was discarded and no further study was made.

Figure 4 shows that the parameter $\alpha 3$, NXP, $l4$ and $l5$ have a clear impact on improving the performance of the ejector and, thus, these four were selected for further analysis.

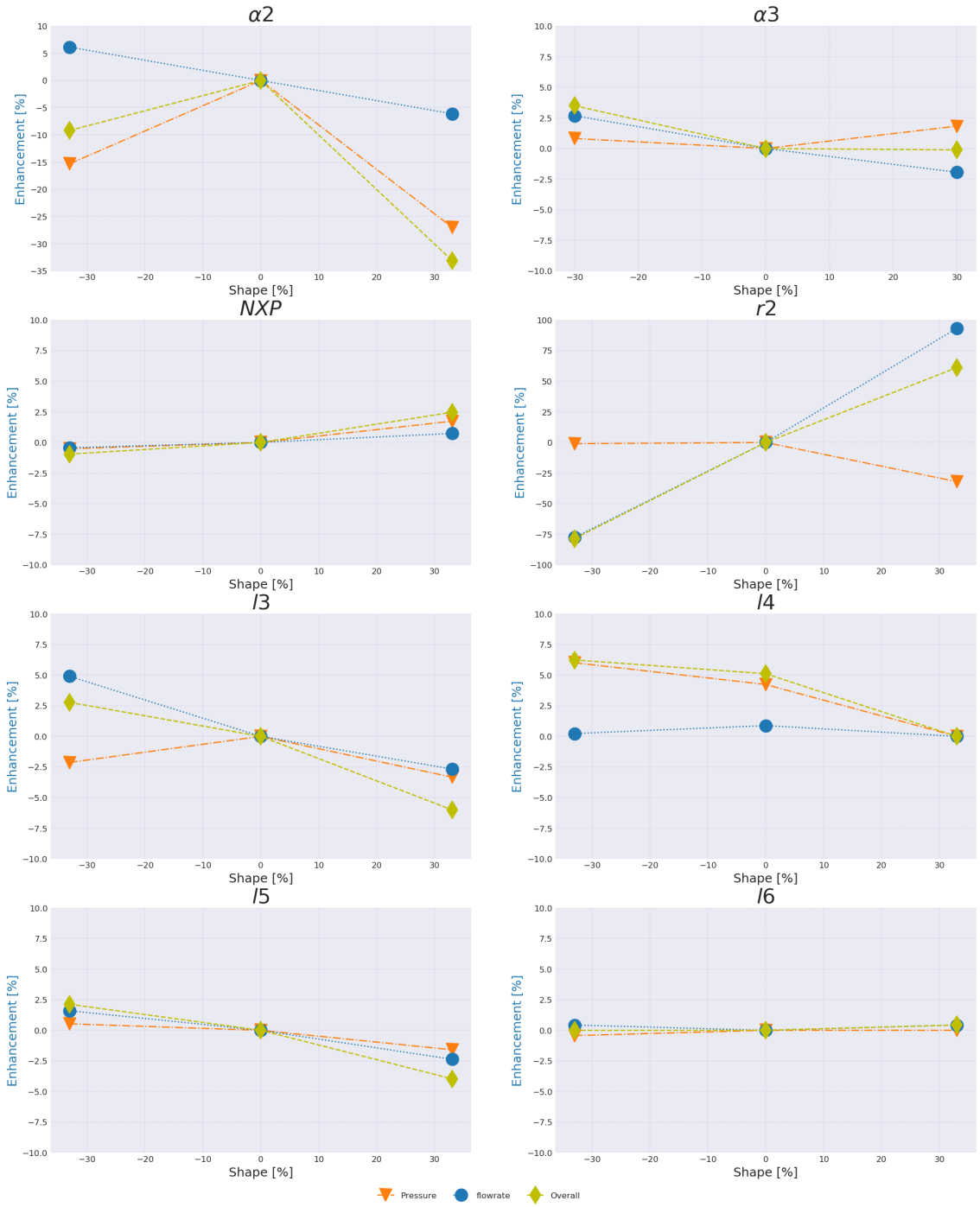

Figure 4. Single influence per each relevant parameter on the flow rate, pressure and overall enhancement of the ejector.

3.1.2. Single-Factor Analysis for the Selected Parameters

The single-factor results are shown in Figure 5.

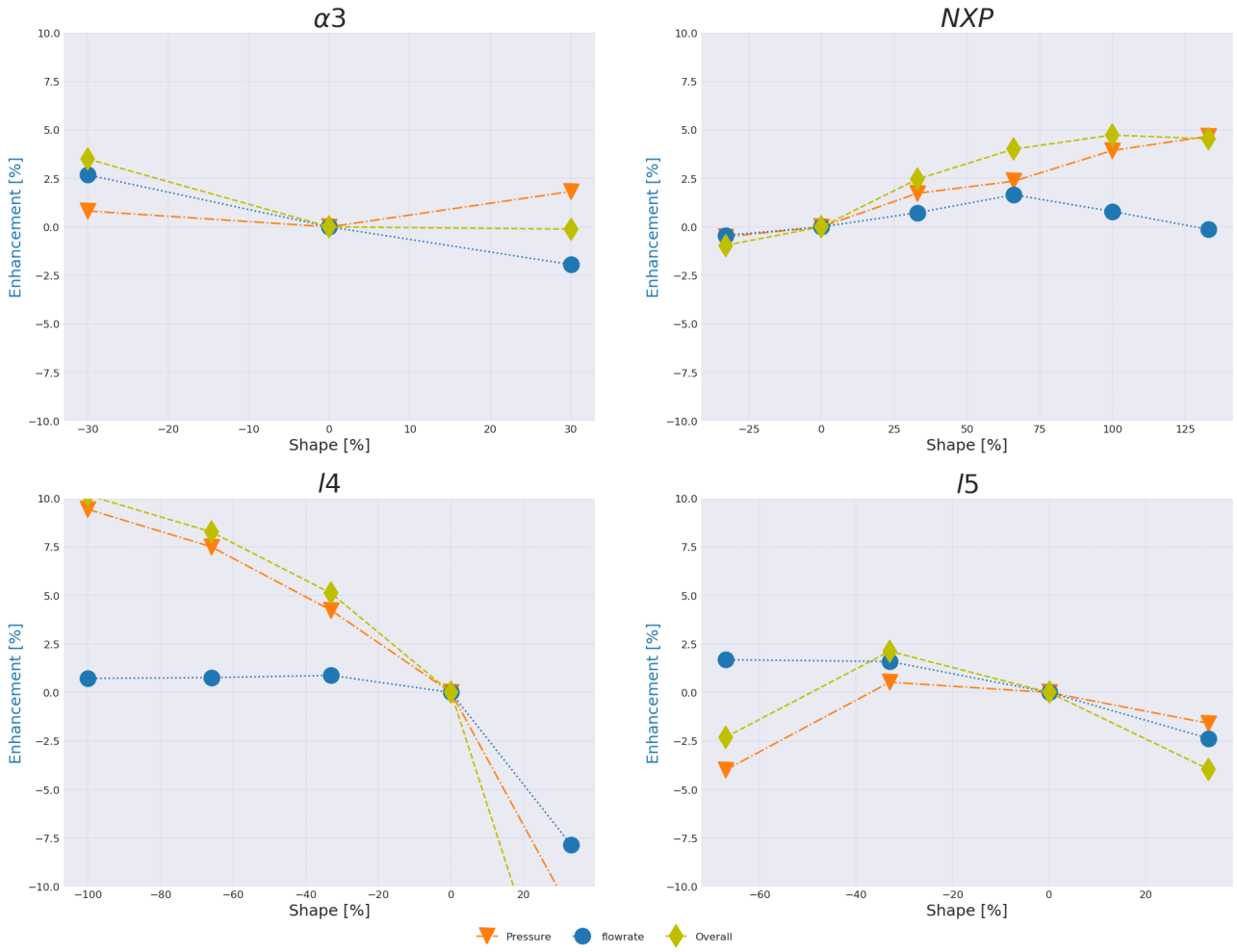

Figure 5. Results on the improvement of the single factor for the selected parameters.

For the construction and evaluation of the new geometries, the method explained in Section 2.2.2 was followed.

For the parameter $\alpha 3$, further investigations of decreasing this parameter will create similar geometries as increasing another parameter in evaluation: the length of the mixing chamber, the l4. Therefore, the study of new geometries for this parameter was concluded at this point. The geometric parameter value shows the maximum single improvement for $-1/3RV$.

For the parameter NXP, exhaustive research has been carried out up to $+133\%RV$ that fails the optimization criterion. The geometric parameter value shows maximum single improvement at $+100\%RV$.

For the parameter $l4$, exhaustive research was carried out up to $-100\%RV$. Thus, the study of new geometries for this parameter was concluded at this point. The geometric parameter value shows maximum single improvement at $-100\%RV$.

For the parameter $l5$, exhaustive research has been carried out up to $-100\%RV$ that fails the optimization criterion. The geometric parameter value shows maximum single improvement at $-2/3RV$.

Table 4 shows the individual enhancement for each parameter on the overall performance.

Table 4. Enhancement per individual values.

Parameter	Original Shape (%)	FR_E (%)	SP_E (%)	O_E (%)
$\alpha 3$	−33	2.7	0.8	3.5
NXP	100	1	3.9	4.9
$l4$	−100	0.6	9.4	10
$l5$	−33	1.9	0.5	2.4

The selected parameters and their two levels are listed in Table 5. Level A is the reference value, and level B is the selected geometrical value.

Table 5. Level A shows the reference value (RV), the start point and level B shows the selected values for each parameter.

Parameter	Level A [1]	Level B
$\alpha 3$	RV	2RV/3
NXP	RV	2RV
$l4$	RV	0
$l5$	RV	1RV/3

[1] Exact values deleted for confidentiality purposes.

The different geometries that show the maximum single enhancement are depicted in Figures 6–9. Figures 6–9 show levels A and B for the four selected parameters, $\alpha 3$, NXP, $l4$ and $l5$.

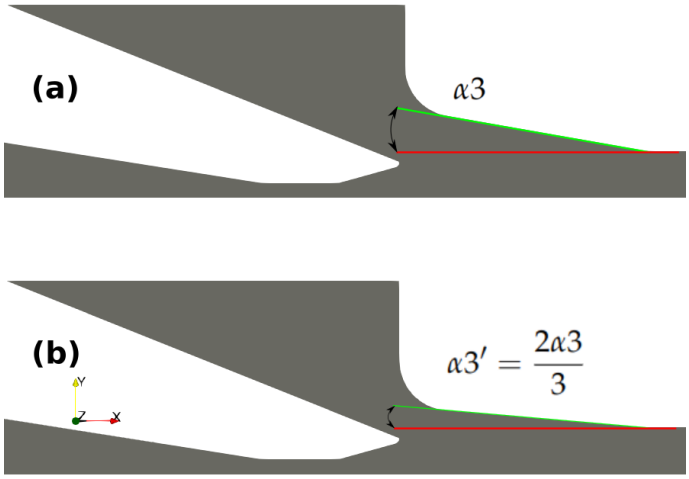

Figure 6. (**a**) $\alpha 3$ with its reference angle; (**b**) $\alpha 3$ when modified.

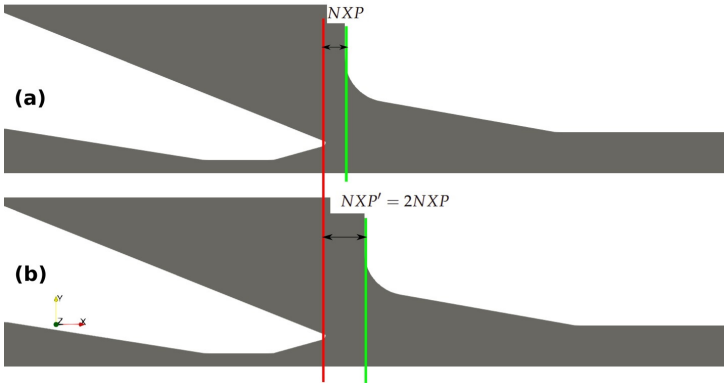

Figure 7. (**a**) NXP with its reference length; (**b**) NXP when modified.

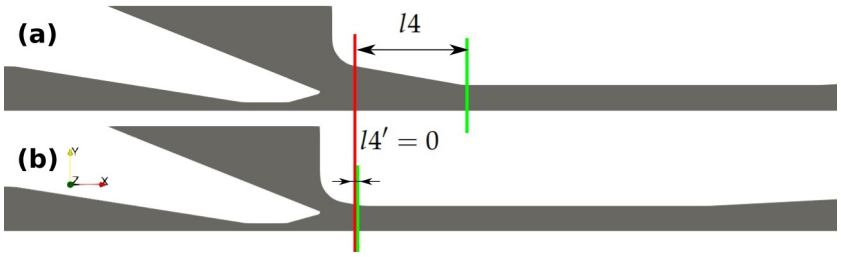

Figure 8. (**a**) *l*4 with its reference length; (**b**) *l*4 when modified.

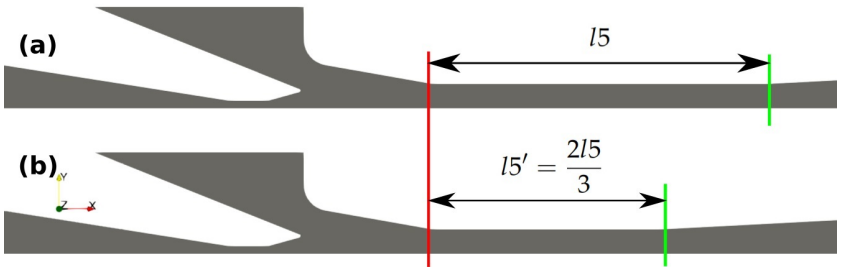

Figure 9. (**a**) *l*5 with its reference length; (**b**) *l*5 when modified.

3.2. Multi-Factor Design Results

The full factorial requires sixteen combinations to examine the influence of each parameter on the overall improvement. Table 6 shows all combinations, parameters and levels, on which the factorial system is based.

Table 6. Full factorial combination design. Both levels, A and B, are shown in Table 5.

Run #	**0**	**1**	**2**	**3**	**4**	**5**	**6**	**7**	**8**	**9**	**10**	**11**	**12**	**13**	**14**	**15**
NXP	A	A	A	A	A	A	A	A	B	B	B	B	B	B	B	B
*l*4	A	A	A	A	B	B	B	B	A	A	A	A	B	B	B	B
*l*5	A	A	B	B	A	A	B	B	A	A	B	B	A	A	B	B
*α*3	A	B	A	B	A	B	A	B	A	B	A	B	A	B	A	B

For the sake of convenience, a fractional factorial design was used and Table 7 shows the number of combinations required.

The eight multi-factor combinations are the result of the fractional factorial design of the four parameters and their two levels per parameter. This fractional factorial design allows us to divide by two the number of combinations but allows capturing the influence per parameter on the overall enhancement.

Table 7. Fractional factorial combination design. Both levels, A and B, are shown in Table 5.

Run #	**0**	**1**	**2**	**3**	**4**	**5**	**6**	**7**	**8**
NXP	A	A	A	A	B	B	B	B	B
*l*4	A	A	B	B	A	A	B	B	B
*l*5	A	A	B	B	B	B	A	A	B
*α*3	A	B	A	B	A	B	A	B	B

Table 8 and Figure 10 show the improvement results for each combination number of the factional factorial design.

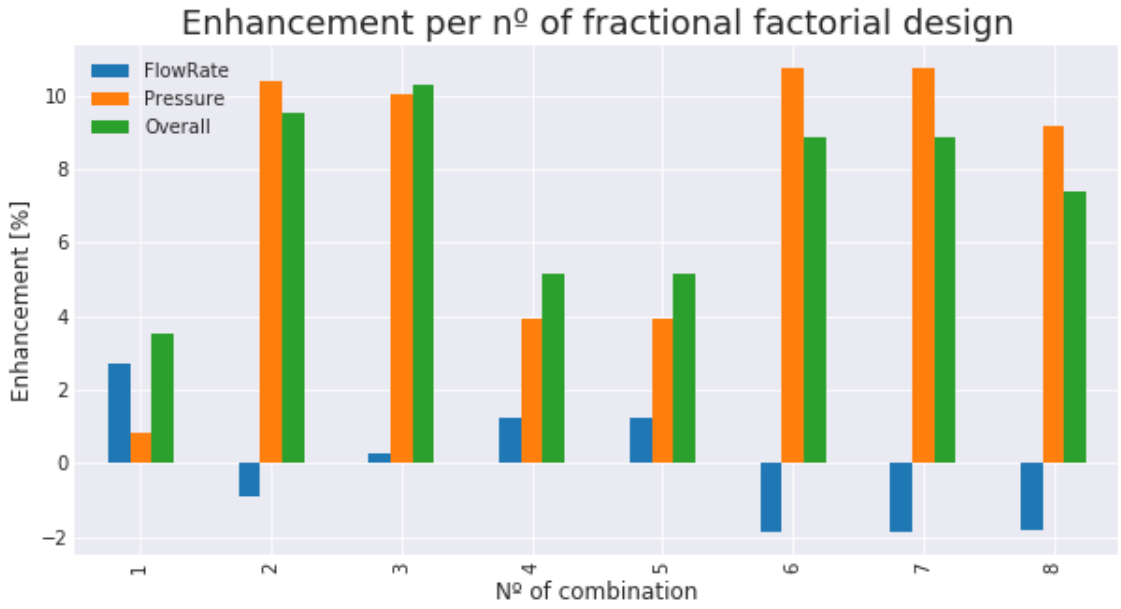

Figure 10. Enhancement per combination number of fractional factorial design.

Table 8. Enhancement per number of the fractional factorial design.

Enhancement	1	2	3	4	5	6	7	8
FR_E (%)	2.7	−0.8	0.4	1.2	1.2	−1.8	−1.8	−1.8
SP_E (%)	0.8	10.4	10	3.9	3.9	10.7	10.7	9.2
O_E (%)	3.5	9.6	10.4	5.2	5.2	8.9	8.9	7.4

In Figure 11, the two simulation results for the geometry constructed with the parameters at the reference values are shown. In Figure 12, the two simulation results for geometry number three of the multi-factor parameters are shown. Geometry number three maximizes the improvement of the performance of the vacuum ejector

Figure 12a suggests that reduction of $l4$ prevents the formation of reflected shock waves in the mixing chamber.

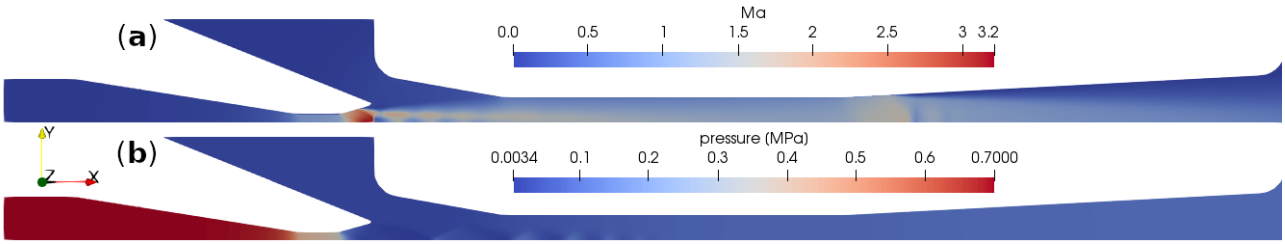

Figure 11. Geometry with the reference values. (**a**) Results for the maximum entrained flow simulation. (**b**) Results for the minimum secondary pressure simulation.

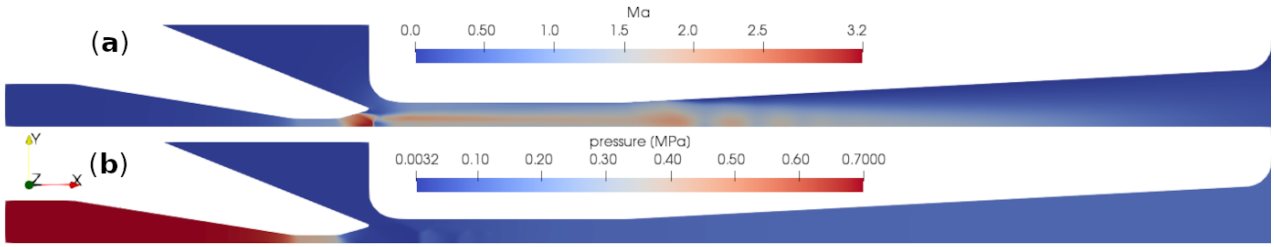

Figure 12. Geometry with the parameter combinations that enhance the performance. (**a**) Results for the maximum entrained flow simulation. (**b**) Results for the minimum secondary pressure simulation.

4. Discussion

Out of thirteen parameters, five have been neglected, giving a total of eight parameters studied. Following a methodology explained in this paper, four parameters out of eight have met the criterion and have shown a good overall improvement in performance by changing their geometric values. In Figure 5, the single enhancement for the four relevant parameters are plotted, and in Table 4 the exact values are shown.

In previous work [1] the ejector with internal geometry of reference values showed an experimental performance of $\mu = 0.992$ and $p_s^* = 0.218$.

Applying the geometric value change for the $\alpha 3$, the flow rate performance is enhanced by $\mu' = (100 + 2.7)\%\mu$ and the pressure performance of the ejector is improved $p_s^{*'} = (100 + 0.8)\%p_s^*$. The actual values are $\mu' = 1.019$ and $p_s^{*'} = 0.209$.

Applying the geometric value change for the NXP, the flow rate performance is enhanced by $\mu' = (100 + 0.8)\%\mu$ and the pressure performance of the ejector is improved $p_s^{*'} = (100 + 9.2)\%p_s^*$. The actual values are $\mu' = 1.004$ and $p_s^{*'} = 0.173$.

Applying the geometric value change for the $l4$, the flow rate performance is enhanced by $\mu' = (100 + 0.6)\%\mu$ and the pressure performance of the ejector is improved $p_s^{*'} = (100 + 9.4)\%p_s^*$. The actual values are $\mu' = 0.999$ and $p_s^{*'} = 0.123$.

Applying the geometric value change for the $l5$, the flow rate performance is enhanced by $\mu' = (100 + 1.6)\%\mu$ and the pressure performance of the ejector is improved $p_s^{*'} = (100 + 0.5)\%p_s^*$. The actual values are $\mu' = 1.008$ and $p_s^{*'} = 0.212$.

A multi-factor design was performed to analyse the improvement of the performance of the ejector with the combination of factors. A fractional factorial design was used because it captures the most relevant combination of parameters with less computational resource utilization.

In Figure 10 the single enhancements for the four relevant parameters are plotted, and in Table 8 the exact values are shown.

The combination of factors numbers two, six, seven and eight fail to accomplish the criteria of optimization described in Section 2.2.1 and, thus, are discarded.

The best-improved performance is when combining all parameters in level B, except NXP, which is at level A.

All combinations where $l4$ is at level B showed a better enhancement in pressure and in overall performance. The influence of the $l4$ parameter on the fractional factorial design is crucial.

Combination number two and number three only differ in the level of $\alpha 3$: first, in level A and second, in level B. Number three shows an improvement in all enhancements analysed compared to number two. The reason for this is because the single influence of the $\alpha 3$ shows the best-entrained flow enhancement, as illustrated in Table 4.

Combination number three on the fractional factorial design shows the best improvement of the performance in both the multi-factor design and single-factor design. Combination number three is made of $NXP' = 2NXP$, $l4' = 0$, $l5' = 2l5/3$ and $\alpha 3' = \alpha 3$. The multi-factor design shows a better improvement over the single-factor design. Although

the combination of factors improves the performance, no significant relevance was detected in the multi-factor improvement over $l4$ length improvement alone.

The entrained flow performance enhanced by the fractional factorial design number three is $\mu' = (100 + 0.3)\%\mu$. Its pressure improved performance of the ejector is $p_s^{*'} = (100 + 10)\%p_s^*$. The actual values are $\mu' = 0.994$ and $p_s^{*'} = 0.117$.

Figure 12 shows overall enhancement over the results in Figure 11, which displays the results with the previous geometry of the ejector.

An enhancement in the overall performance of the supersonic vacuum ejector was achieved by means of changing the internal geometry.

5. Conclusions

The aim of the present paper has been successfully achieved with a substantial margin of improvement.

Out of thirteen initial geometrical parameters, five were discarded based on industrial criteria and eight were chosen for study. After setting an improvement criterion, a trial and error plan was followed in which the geometric values of each parameter were modified from their reference value. Two new geometries were created and two simulations were carried out for each geometry.

Consequently, from the last eight parameters, four parameters were selected for further evaluation in a single-factor evaluation. The selected parameters are $\alpha 3$, NXP, $l4$ and $l5$ and the single-factor analysis shows that the modified values of their geometrical reference values are, $\alpha 3 = -1/3RV$, $NXP = 2RV$, $l4 = 0$ and $l5 = -1/3RV$. Additionally, the individual overall enhancements per parameter are $\alpha 3 = +3.5\%$, $NXP = +4.9\%$, $l4 = +10\%$ and $l5 = +2.4\%$. The best single performance enhancement is $+10\%$ and is produced by changing the geometrical value of $l4$.

As a further step, a multi-factor analysis was performed to find the combination of the parameters that improves the whole performance of the ejector. A fractional factorial design, based on a fractional designed experiment, was proposed. This design is capable of exhibiting the influence of all four parameters on the overall enhancement by forcing variability to occur and then determining optimal control factor settings.

There are four parameters and two levels per parameter: level A, the reference value, and level B, the proposed one.

Combination number three is made up of the combination of all parameters in level B, except the distance between nozzles. This combination of parameters shows the best improvement of the performance of the ejector by an overall enhancement of 10.4%, including a positive enhancement in both the entrained flow and in the secondary pressure.

Although the combination of factors improves the performance, no significant relevance has been detected in the multi-factor improvement over the $l4$ length single-factor improvement. However, as this tool is widely used, a small improvement in its performance means an important energy saving.

In future work, the geometric configuration of the Laval ejector nozzle will be evaluated, as the literature suggests there may be further improvement.

Author Contributions: Conceptualization, L.M.; methodology, L.M. and R.C.; software, R.C.; validation, P.J.G.-M., G.R. and R.C.; formal analysis, P.J.G.-M. and R.C.; investigation, L.M.; resources, R.C.; data curation, L.M., G.R., R.C. and P.J.G.-M.; writing—original draft preparation, L.M.; writing—review and editing, G.R., P.J.G.-M. and R.C.; visualization, L.M.; supervision, G.R., R.C. and P.J.G.-M.; project administration, R.C. All authors have read and agreed to the published version of the manuscript.

Funding: This research received external funding from Generalitat de Catalunya. Support of Industrial Doctorate (2018 DI 025) from Generalitat de Catalunya is acknowledged.

Institutional Review Board Statement: Not applicable.

Informed Consent Statement: Not applicable.

Data Availability Statement: For interpretation of the references to colour in the figures' legend this paper has, the reader is referred to the Web version of this article.

Conflicts of Interest: The authors declare no conflict of interest.

Abbreviations

The following abbreviations are used in this manuscript:

A	Area
$\alpha 1$	Convergent angle of the first nozzle (º)
$\alpha 2$	Divergent angle of the first nozzle (º)
$\alpha 3$	Convergent angle of the second nozzle (º)
$\alpha 4$	Divergent angle of the second nozzle (º)
c_v	Specific heat at constant volume (J/kg K)
C_p	Specific heat capacity at constant pressure (J/kg K)
FR_E	Secondary flow rate enhancement (%)
$l1$	Horizontal distance for the convergent section of the first nozzle (mm)
$l2$	Horizontal distance for the throat section of the first nozzle (mm)
$l3$	Horizontal distance for the divergent section of the first nozzle (mm)
$l4$	Horizontal distance for the mixing chamber section of the second nozzle (mm)
$l5$	Horizontal distance for the constant area section of the second nozzle (mm)
$l6$	Horizontal distance for the diffuser section of the second nozzle (mm)
$\dot{m}_p$	Primary flow rate (kg/s)
$\dot{m}_s$	Secondary flow rate (kg/s)
M	Molecular mass (g/mol)
μ	Normalized entrained flow ratio (-)
μ_0	Dynamic viscosity (kg/s m)
NXP	Nozzle exit position (mm)
O_E	Overall enhancement (%)
p_a	Atmospheric pressure (Pa)
p_s^*	Normalized secondary pressure (-)
p_s	Pressure in secondary inlet (Pa)
$r1$	Radius for the throat of the first nozzle (mm)
$r2$	Radius for the throat of the second nozzle (mm)
ρ	Density (kg/m^3)
R'	Constant for gases (J/mol K)
RV	Reference value
SP_E	Secondary pressure enhancement (%)
T	Temperature (K)
$\lvert\mathbf{u}\rvert$	Magnitude of velocity
$u_{i,j}$	Velocity components in directions i and j (m/s)

References

1. Macia, L.; Castilla, R.; Gamez-Montero, P.J.; Camacho, S.; Codina, E. Numerical Simulation of a Supersonic Ejector for Vacuum Generation with Explicit and Implicit Solver in Openfoam. *Energies* **2019**, *12*, 3553. [CrossRef]
2. Besagni, G.; Mereu, R.; Inzoli, F. Ejector refrigeration: A comprehensive review. *Renew. Sustain. Energy Rev.* **2016**, *53*, 373–407. [CrossRef]
3. Arun Kumar, R.; Rajesh, G. Physics of vacuum generation in zero-secondary flow ejectors. *Phys. Fluids* **2018**, *30*, 066102. [CrossRef]
4. Lamberts, O.; Chatelain, P.; Bartosiewicz, Y. New methods for analyzing transport phenomena in supersonic ejectors. *Int. J. Heat Fluid Flow* **2017**, *64*, 23–40. [CrossRef]
5. Jafarian, A.; Azizi, M.; Forghani, P. Experimental and numerical investigation of transient phenomena in vacuum ejectors. *Energy* **2016**, *102*, 528–536. [CrossRef]
6. Goodman, N.; Leege, B.J.; Johnson, P.E. An improved de Laval nozzle experiment. *Int. J. Mech. Eng. Educ.* **2021**, *50*, 513–537. [CrossRef]
7. Duan, Z.; Ma, Z.; Guo, Y.; Zhang, J.; Sun, S.; Liang, L. Study on Supersonic Dehydration Efficiency of High Pressure Natural Gas. *Sustainability* **2020**, *12*, 488. [CrossRef]
8. Dong, J.; Hu, Q.; Yu, M.; Han, Z.; Cui, W.; Liang, D.; Ma, H.; Pan, X. Numerical investigation on the influence of mixing chamber length on steam ejector performance. *Appl. Therm. Eng.* **2020**, *174*, 115204. [CrossRef]

9. Yan, J.; Li, S.; Liu, Z. Numerical investigation on optimization of ejector primary nozzle geometries with fixed/varied nozzle exit position. *Appl. Therm. Eng.* **2020**, *175*, 115426. [CrossRef]
10. Yan, J.; Li, S.; Li, R. Numerical study on the auxiliary entrainment performance of an ejector with different area ratio. *Appl. Therm. Eng.* **2021**, *185*, 116369. [CrossRef]
11. Zhang, H.; Wang, L.; Jia, L.; Wang, X. Assessment and prediction of component efficiencies in supersonic ejector with friction losses. *Appl. Therm. Eng.* **2018**, *129*, 618–627. [CrossRef]
12. Karthick, S.K.; Rao, S.M.; Jagadeesh, G.; Reddy, K.P. Parametric experimental studies on mixing characteristics within a low area ratio rectangular supersonic gaseous ejector. *Phys. Fluids* **2016**, *28*, 076101. [CrossRef]
13. Zhang, K.; Shen, S.; Yang, Y.; Tian, X. Experimental Investigation of Adjustable Ejector Performance. *J. Energy Eng.* **2011**, *138*, 125–129. [CrossRef]
14. Ramesh, A.S.; Sekhar, S.J. Experimental and numerical investigations on the effect of suction chamber angle and nozzle exit position of a steam-jet ejector. *Energy* **2018**, *164*, 1097–1113. [CrossRef]
15. Ramesh, A.S.; Joseph Sekhar, S. Experimental studies on the effect of suction chamber angle on the entrainment of passive fluid in a steam ejector. *J. Fluids Eng. Trans. ASME* **2018**, *140*, 011106. [CrossRef]
16. Van Nguyen, V.; Varga, S.; Soares, J.; Dvorak, V.; Oliveira, A.C. Applying a variable geometry ejector in a solar ejector refrigeration system. *Int. J. Refrig.* **2020**, *113*, 187–195. [CrossRef]
17. Riaz, F.; Tan, K.H.; Farooq, M.; Imran, M.; Lee, P.S. Energy Analysis of a Novel Ejector-Compressor Cooling Cycle Driven by Electricity and Heat (Waste Heat or Solar Energy). *Sustainability* **2020**, *12*, 8178. [CrossRef]
18. Sierra-Pallares, J.; García del Valle, J.; Paniagua, J.M.; García, J.; Méndez-Bueno, C.; Castro, F. Shape optimization of a long-tapered R134a ejector mixing chamber. *Energy* **2018**, *165*, 422–438. [CrossRef]
19. Wu, Y.; Zhao, H.; Zhang, C.; Wang, L.; Han, J. Optimization analysis of structure parameters of steam ejector based on CFD and orthogonal test. *Energy* **2018**, *151*, 79–93. [CrossRef]
20. OpenFOAM Foundation. OpenFOAM User Guide: CFD Direct. Architects of OpenFOAM. Available online: https://cfd.direct/openfoam/user-guide/ (accessed on 31 May 2022).
21. Heyns, J.A.; Oxtoby, O.F.; Steenkamp, A. HiSA. Available online: https://hisa.gitlab.io/ (accessed on 31 May 2022).
22. Heyns, J.A.; Oxtoby, O.F.; Steenkamp, A. (PDF) Modelling high-speed viscous flow in OpenFOAM®. In Proceedings of the 9th OpenFOAM Workshop , Zagreb, Croatia, 23–26 June 2014 .
23. Moukalled, F.; Mangani, L.; Darwish, M. *The Finite Volume Method in Computational Fluid Dynamics*; Springer: Berlin/Heidelberg, Germany, 2016; Volume 113. [CrossRef]
24. Blazek, J. Computational Fluid Dynamics: Principles and Applications: Third Edition. In *Computational Fluid Dynamics: Principles and Applications*, 3rd ed.; Elsevier: Amsterdam, The Netherlands, 2015; pp. 1–447. [CrossRef]
25. Mazzelli, F.; Little, A.B.; Garimella, S.; Bartosiewicz, Y. Computational and experimental analysis of supersonic air ejector: Turbulence modeling and assessment of 3D effects. *Int. J. Heat Fluid Flow* **2015**, *56*, 305–316. [CrossRef]
26. GitHub—Takaakiaoki/Ofblockmeshdicthelper: Helper Utilities for OpenFOAM BlockMeshDict Generation. Available online: https://github.com/takaakiaoki/ofblockmeshdicthelper (accessed on 31 May 2022).
27. Fu, W.; Liu, Z.; Li, Y.; Wu, H.; Tang, Y. Numerical study for the influences of primary steam nozzle distance and mixing chamber throat diameter on steam ejector performance. *Int. J. Therm. Sci.* **2018**, *132*, 509–516. [CrossRef]
28. Chen, H.; Zhu, J.; Ge, J.; Lu, W.; Zheng, L. A cylindrical mixing chamber ejector analysis model to predict the optimal nozzle exit position. *Energy* **2020**, *208*, 118302. [CrossRef]
29. Wang, L.; Liu, J.; Zou, T.; Du, J.; Jia, F. Auto-tuning ejector for refrigeration system. *Energy* **2018**, *161*, 536–543. [CrossRef]
30. Casey, M.; Wintergerste, T. *ERCOFTAC Special Interest Group on "Quality and Trust in Industrial CFD" Best Practice Guidelines*; ERCOFTAC: London, UK, 2000; pp. 1–94.
31. Celik, I.B.; Ghia, U.; Roache, P.J.; Freitas, C.J.; Coleman, H.; Raad, P.E. Procedure for estimation and reporting of uncertainty due to discretization in CFD applications. *J. Fluids Eng. Trans. ASME* **2008**, *130*, 0780011–0780014. [CrossRef]
32. Ballantyne, K.N.; van Oorschot, R.A.; Mitchell, R.J. Reduce optimisation time and effort: Taguchi experimental design methods. *Forensic Sci. Int. Genet. Suppl. Ser.* **2008**, *1*, 7–8. [CrossRef]